

## Dynamic simulation of a multi-cable driven parallel suspension platform with slack cables

Wang, Yandong; Cao, Guohua; van Horssen, Wim T.

**DOI**

[10.1016/j.mechmachtheory.2018.04.014](https://doi.org/10.1016/j.mechmachtheory.2018.04.014)

**Publication date**

2018

**Document Version**

Final published version

**Published in**

Mechanism and Machine Theory

**Citation (APA)**

Wang, Y., Cao, G., & van Horssen, W. T. (2018). Dynamic simulation of a multi-cable driven parallel suspension platform with slack cables. *Mechanism and Machine Theory*, 126, 329-343. <https://doi.org/10.1016/j.mechmachtheory.2018.04.014>

**Important note**

To cite this publication, please use the final published version (if applicable). Please check the document version above.

**Copyright**

Other than for strictly personal use, it is not permitted to download, forward or distribute the text or part of it, without the consent of the author(s) and/or copyright holder(s), unless the work is under an open content license such as Creative Commons.

**Takedown policy**

Please contact us and provide details if you believe this document breaches copyrights. We will remove access to the work immediately and investigate your claim.

***Green Open Access added to TU Delft Institutional Repository***

***'You share, we take care!' - Taverne project***

**<https://www.openaccess.nl/en/you-share-we-take-care>**

Otherwise as indicated in the copyright section: the publisher is the copyright holder of this work and the author uses the Dutch legislation to make this work public.



## Research paper

## Dynamic simulation of a multi-cable driven parallel suspension platform with slack cables

Yandong Wang<sup>a,b</sup>, Guohua Cao<sup>a,\*</sup>, Wim T. van Horssen<sup>b</sup><sup>a</sup> School of Mechatronic Engineering, China University of Mining and Technology, Xuzhou 221116, China<sup>b</sup> Department of Mathematical Physics, Delft Institute of Applied Mathematics, Delft University of Technology, Mekelweg 4, Delft 2628 CD, The Netherlands

## ARTICLE INFO

## Article history:

Received 30 January 2018

Revised 23 March 2018

Accepted 16 April 2018

Available online 27 April 2018

## Keywords:

Non-smooth cable vibrations

Slack cable

Multi-cable driven manipulators

Non-smooth generalized- $\alpha$  scheme

## ABSTRACT

In this paper, a modelling method and an accurate numerical procedure are presented to simulate the dynamical responses of a multi-cable driven parallel suspension platform system. For such systems, the cables might become slack due to external excitations and due to the fact that cables can become tensionless when been pushed in longitudinal direction. In lateral and torsional directions, the constraint forces between the cables and platform can be positive as well as negative. This paper will deal with the non-smooth cable vibrations (in longitudinal, lateral and torsional directions) by taking into account the slackness of the cables. Firstly, the Lagrange equation with constraints is used to derive the equations of motion of the multi-cable suspension platform. Then, by expressing the equations of motion and constraint equations at velocity level, a non-smooth algorithm is used to numerically solve the equations. Finally, the numerical results are compared with an ADAMS simulation, and the two results agree well with each other. Moreover, the results in this paper significantly improve the numerical results used in the analysis of the dynamics for multi-cable systems which usually neglect the lateral properties of the cables.

© 2018 Elsevier Ltd. All rights reserved.

## 1. Introduction

A multi-cable driven parallel suspension platform, which acts as a working platform for workers and carries machines when constructing vertical shafts, mainly consists of three components: a platform, several suspension cables and winding winches [1], as shown in Fig. 1. Due to the flexibility of the suspension cables and their interactions, complicated dynamical phenomena can occur when the platform is lifted up or lowered down. When the cable length is not perfectly controlled, for example, one of the cables can become longer due to the driving error of its drum, and then this cable may become slack because of its unilateral bearing property (can only be pulled) in axial direction [2]. And, when it becomes tensioned again, a shock will be acting on the platform due to the cable state change.

When investigating cable vibrations in single-cable hoisting systems, usually the cable is modelled as a continuum and the governing equations of the system are derived mostly by Hamilton's principle [3,4]. By using various spatial discretization methods, such as a single-mode approximation [5], a Rayleigh–Ritz procedure [6], a Galerkin's method [7,8], the assumed mode method [9], and the method of Lagrange equations [10,11], the derived governing equations can be discretized into ordinary differential equations (ODEs) or differential algebraic equations (DAEs) [12,13], which then can be solved with

\* Corresponding author.

E-mail address: [caoguohua@cumt.edu.cn](mailto:caoguohua@cumt.edu.cn) (G. Cao).

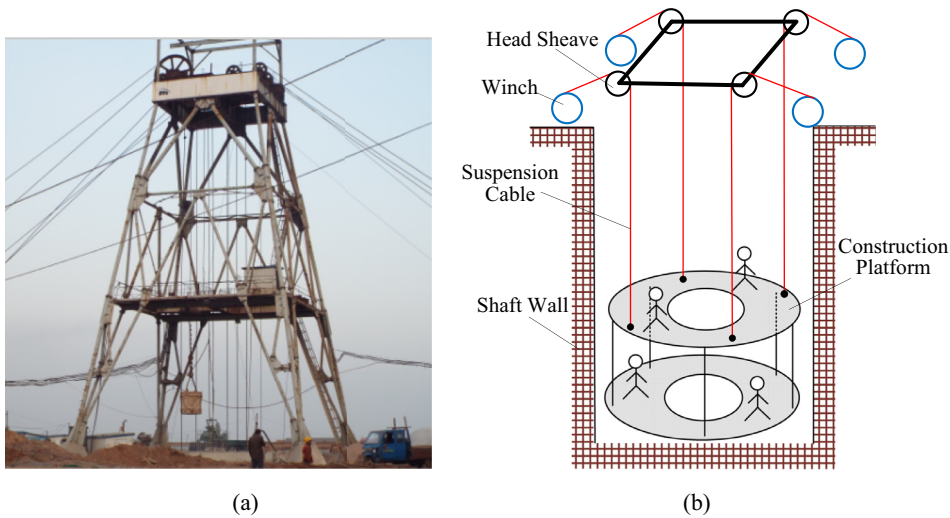


Fig. 1. Multi-cable driven parallel suspension platform system.

numerical methods. Single cable vibration problems can also be solved analytically. Sandilo and van Horsen [14,15] employed a multiple-timescales perturbation method to construct formal asymptotic approximations to the solutions. Gaiko and van Horsen [16] and Akkaya and van Horsen [17] used the method of d'Alembert to obtain the exact lateral response of travelling strings. Laplace transform methods [18,19] can also be used to solve cable vibration problems analytically.

When investigating the dynamics of multi-cable-driven parallel mechanisms, cables in such systems are often simplified as linear [20] or nonlinear [21] springs, or just represented by force vectors [22], while the mechanical properties of the cables are ignored, which implies that the interaction between the cable and the suspended subject cannot be analysed correctly. When considering the unilateral bearing properties of the cables, Shao et al. [2] established a dynamic model of the shaft construction platform by treating the cables as massless, undamped, and perfectly stiff. He transformed the dynamic equations to a linear complementary problem (LCP) and derived the non-smooth dynamical response of the system by solving this LCP based on Lemke's algorithm [23]. However, since only the longitudinal character of the cables is considered, the dynamic responses of the system are not accurately simulated, especially in torsional direction. Moreover, when the cable is relatively long, the lateral oscillations of the cables will have a great effect on the platform (and sometimes called end effector in robotics) [1]. So, the lateral properties of the cables should also be included when investigating the dynamic responses of those systems.

For the multibody systems, when studying the contact behaviour between two rigid bodies, non-smooth time integration methods together with the help of an impact law can be used to deal with the impacts and velocity jumps due to the unilateral constraints [24–26]. Here, we can use those ideas to treat the cable state change (slack versus tensioned) as a “contact” problem and solve it numerically with the non-smooth dynamic theory. In this paper, the non-smooth dynamical model of the multi-cable parallel suspension platform is established. By including the longitudinal, in-plane and the out-of-plane lateral, torsional and longitudinal-torsional coupled mechanical character of the cable, as well as its slackness, the equations of motion are derived using Lagrange's principle. Then, by modifying the complementary condition of a non-smooth generalized- $\alpha$  scheme [25] and, by using this in the derived differential algebraic equations, the non-smooth responses of the system are obtained numerically. Finally, the numerical results of the modified algorithm are compared with an ADAMS simulation. The two results agree well with each other, which confirms the validity of the presented numerical method. The method presented in this paper provides a more accurate way to simulate the dynamic responses of multi-cable driven manipulators, such as a multi-crane lifting system, or a parallel cable robot, etc. The presented method also shows in general how cable non-smooth dynamical responses can accurately be investigated.

## 2. Dynamic model and equations of motion

### 2.1. Description of the system

First of all, several assumptions are made here to restrict the analysis:

- Since the cable bending stiffness is quite small [7], it is neglected in this paper.
- Due to the slowly varying cable length, low longitudinal excitation frequencies and the large longitudinal stiffness of the catenary part, it is assumed that the catenary will always behave like a rigid body. So the catenary has no influence on the vertical part and is neglected in this paper, as well as the motion of the head-sheave;

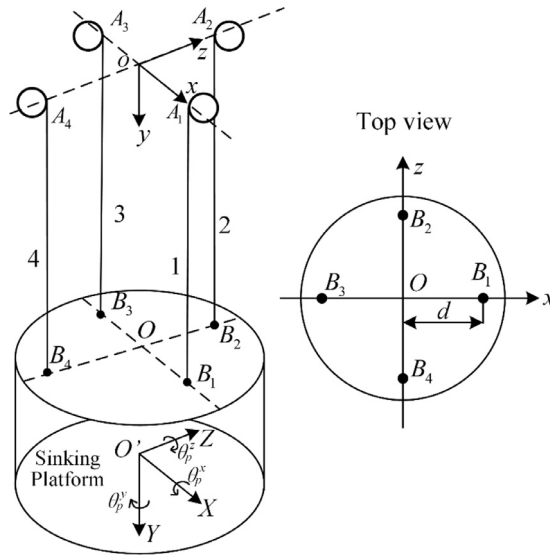


Fig. 2. Four-cable driven parallel suspension platform.

- The mass per unit length (in kg/m) is denoted by  $\rho$ , and  $J_c$  the moment of inertia per unit length (in kg m) of the cable. Both are assumed to be uniform.

By the assumptions made above, the diagram of a four-cable driven parallel suspension platform system is simplified and shown in Fig. 2, where  $A_i$  is the tangent point between cable  $i$  and head sheave  $i$ , and  $B_i$  is the connecting point between cable  $i$  and the platform, where  $i = 1, 2, 3, 4$ . The cables are arranged symmetrically and the tangent points form a square  $A_1A_2A_3A_4$ , whose centroid point  $o$  is used to define the coordinate frame  $oxyz$ . Similarly, the centroid of the square  $B_1B_2B_3B_4$  is denoted by  $O$ , and the length of  $OB_i$  is  $d$ . A local frame  $O'XYZ$  is defined at the platform mass centre  $O'$ . The prescribed length of all the cables is denoted by  $l(t)$ , and the displacement excitations of cable  $i$  at point  $A_i$  in three directions are given by  $e_i^x(t)$ ,  $e_i^y(t)$  and  $e_i^z(t)$ , respectively, where  $t$  is time. The prescribed velocity and acceleration will be denoted by  $v(t)$  and  $a(t)$ , respectively. The longitudinal and torsional dynamic displacement of cable  $i$  at position  $y$  and at time  $t$  is  $u_i(y, t)$  and  $\theta_i(y, t)$ , respectively, and the lateral dynamic displacement of cable  $i$  in  $x$ - and  $z$ - directions are  $w_i^x(y, t)$  and  $w_i^z(y, t)$ , respectively. The real length of cable  $i$  can be expressed as

$$l_i(t) = l(t) + e_i^y(t) + u_i(l(t), t), \tag{1}$$

and the position and the angle of the platform are given by

$$\begin{bmatrix} w_p^x(t) & l(t) + u_p(t) & w_p^z(t) & \theta_p^x(t) & \theta_p^y(t) & \theta_p^z(t) \end{bmatrix}, \tag{2}$$

where  $u_p(t)$ ,  $w_p^x(t)$  and  $w_p^z(t)$  are the dynamical displacements of the platform in  $y$ -,  $x$ - and  $z$ -directions, while  $\theta_p^x(t)$ ,  $\theta_p^y(t)$  and  $\theta_p^z(t)$  are the orientation angles of the platform about the  $X$ -,  $Y$ - and  $Z$ -axis at time  $t$ .

In the longitudinal direction, since the cable length of cable  $i$  is always larger or equal to  $|A_iB_i|$ , which is the distance between  $A_i$  and  $B_i$ , the constraint for the cable  $i$  and the platform will be

$$\psi_i^u(t) = l_i(t) - |A_iB_i| \geq 0. \tag{3}$$

Since the lateral and the torsional displacement of the platform are quite small compared to the cable length,  $|A_iB_i|$  can be approximated by the  $y$  coordinate value of  $B_i$ . In the lateral and torsional direction, the dynamic displacement of the lower end of the cable will always be equal to its connecting point to the platform. With those notations, the constraint equations between the cables and the platform can be expressed as

$$\psi = \left[ (\psi^u)^T (\psi^b)^T \right]^T, \tag{4}$$

where the constraint equations are

$$\psi^u(t) = \begin{bmatrix} u_1(l(t), t) + e_1^y(t) - (u_p(t) + d \cdot \sin(\theta_p^z(t))) \geq 0 \\ u_2(l(t), t) + e_2^y(t) - (u_p(t) - d \cdot \sin(\theta_p^x(t))) \geq 0 \\ u_3(l(t), t) + e_3^y(t) - (u_p(t) - d \cdot \sin(\theta_p^z(t))) \geq 0 \\ u_4(l(t), t) + e_4^y(t) - (u_p(t) + d \cdot \sin(\theta_p^x(t))) \geq 0 \end{bmatrix}, \tag{5}$$

and where the constraints for the cables and the platform in torsional and lateral directions are

$$\psi^b(t) = \left[ (\psi^b_T(t))^T (\psi^b_L(t))^T \right]^T, \tag{6}$$

in which

$$\begin{aligned} \psi^b_{T,i}(t) &= \theta_i(l(t), t) - \theta^y_p(t) = 0, \\ \psi^b_{L,1}(t) &= \begin{bmatrix} w^x_1(l(t), t) - w^x_p(t) - c \cdot \theta^z_p = 0 \\ w^z_1(l(t), t) - w^z_p(t) + c \cdot \theta^x_p + d \cdot \theta^y_p = 0 \end{bmatrix}, \\ \psi^b_{L,2}(t) &= \begin{bmatrix} w^x_2(l(t), t) - w^x_p(t) - c \cdot \theta^z_p - d \cdot \theta^y_p = 0 \\ w^z_2(l(t), t) - w^z_p(t) + c \cdot \theta^x_p = 0 \end{bmatrix}, \\ \psi^b_{L,3}(t) &= \begin{bmatrix} w^x_3(l(t), t) - w^x_p(t) - c \cdot \theta^z_p = 0 \\ w^z_3(l(t), t) - w^z_p(t) + c \cdot \theta^x_p - d \cdot \theta^y_p = 0 \end{bmatrix}, \\ \psi^b_{L,4}(t) &= \begin{bmatrix} w^x_4(l(t), t) - w^x_p(t) - c \cdot \theta^z_p + d \cdot \theta^y_p = 0 \\ w^z_4(l(t), t) - w^z_p(t) + c \cdot \theta^x_p = 0 \end{bmatrix}, \end{aligned} \tag{7}$$

where  $c$  is the distance measured from the barycentre of the platform to its top.

Denoting the mass of the platform by  $m_p$ , the moment of inertia of the platform about the three axes by  $J^x_p$ ,  $J^y_p$  and  $J^z_p$ , respectively, the kinetic energy of the system can be expressed as

$$\begin{aligned} K &= \sum_{i=1}^4 \int_0^{l(t)} \frac{1}{2} \rho \left[ v_i(t) + \frac{Du_i(y, t)}{Dt} \right]^2 dy + \sum_{i=1}^4 \int_0^{l(t)} \frac{1}{2} J_c \left[ \frac{D\theta_i(y, t)}{Dt} \right]^2 dy \\ &+ \dots \sum_{i=1}^4 \frac{1}{2} \rho \int_0^{l(t)} \left[ \left( \frac{Dw^x_i(y, t)}{Dt} \right)^2 + \left( \frac{Dw^z_i(y, t)}{Dt} \right)^2 \right] dy + \dots \\ &\times \frac{1}{2} m_p \left[ (v(t) + \dot{u}_p(t))^2 + (\dot{w}^x_p(t))^2 + (\dot{w}^z_p(t))^2 \right] + \dots \frac{1}{2} J^x_p (\dot{\theta}^x_p(t))^2 + \frac{1}{2} J^y_p (\dot{\theta}^y_p(t))^2 + \frac{1}{2} J^z_p (\dot{\theta}^z_p(t))^2, \end{aligned} \tag{8}$$

where an over dot denotes the derivative with respect to  $t$ , and the operator  $\frac{D}{Dt}$  is defined by

$$\frac{D}{Dt} = \frac{\partial}{\partial t} + v(t) \frac{\partial}{\partial y}. \tag{9}$$

Taking the longitudinal-torsional coupled mechanical properties of the cables into consideration, the potential energy of the system is

$$\begin{aligned} U &= \sum_{i=1}^4 \int_0^{l(t)} \left[ \left( T_{c,i}(y, t) + \frac{1}{2} T_{d,i}(y, t) \right) \frac{\partial u_i(y, t)}{\partial y} + \left( M_{c,i}(y, t) + \frac{1}{2} M_{d,i}(y, t) \right) \frac{\partial \theta_i(y, t)}{\partial y} \right] dy + \dots \\ &\times \sum_{i=1}^4 \left[ \int_0^{l(t)} \frac{1}{2} T_{c,i} \left[ \left( \frac{\partial w^x_i(y, t)}{\partial y} \right)^2 + \left( \frac{\partial w^z_i(y, t)}{\partial y} \right)^2 \right] dy - \rho g(y + u_i(y, t)) \right] + \dots - m_p g(l(t) + u_c(t)), \end{aligned} \tag{10}$$

where  $g$  is the gravitational acceleration,  $T_{c,i}(y, t) = m_p g/4 + \rho(l(t) - y)g$  and  $T_{d,i}(y, t) = Q_1 \cdot \partial u_i(y, t)/\partial y + Q_{2,i} \cdot \partial \theta_i(y, t)/\partial y$  are the static and dynamic axial tension of cable  $i$  at position  $y$  at time  $t$ ,  $M_{c,i}(y, t) = Q_{3,i}/Q_1 \cdot T_{c,i}(y, t)$  and  $M_{d,i}(y, t) = Q_{3,i} \cdot \partial u_i(y, t)/\partial y + Q_4 \cdot \partial \theta_i(y, t)/\partial y$  are the static and dynamic torque of cable  $i$  at position  $y$  at time  $t$ .  $Q_1$  and  $Q_4$  are the longitudinal and torsional stiffness of the cables, respectively,  $Q_{2,i}$  and  $Q_{3,i}$  are the longitudinal-torsional coupled stiffness of cable  $i$  (see also [27]), respectively. Since  $Q_{2,i}$  approximates  $Q_{3,i}$ , a new parameter  $Q_{23,i}$  is introduced to represent those two parameters.

### 2.2. Equation of motion

The transformation  $\xi = y/l(t)$  is used to transform the time-varying domain  $[0, l(t)]$  for  $y$  to a fixed one  $[0, 1]$  for  $\xi$ . The new dependent variables can be expressed as

$$\bar{u}_i(\xi, t) = u_i(y, t), \quad \bar{w}^x_i(\xi, t) = w^x_i(y, t), \quad \bar{w}^z_i(\xi, t) = w^z_i(y, t), \quad \bar{\theta}_i(\xi, t) = \theta_i(y, t), \tag{11}$$

and their partial derivatives with respect to  $\xi$  and  $t$  will become

$$\frac{\partial V_O(y, t)}{\partial y} = \frac{1}{l(t)} \frac{\partial V_N(\xi, t)}{\partial \xi}, \quad \frac{\partial V_O(y, t)}{\partial t} = \frac{\partial V_N(\xi, t)}{\partial t} + \frac{v(t)\xi}{l(t)} \frac{\partial V_N(\xi, t)}{\partial \xi}, \tag{12}$$

in which  $V_O(x, t)$  denotes the old variables and  $V_N(\xi, t)$  denotes the new ones.

By using the assumed mode method (see also [28]), the dynamic displacements can be approximated by

$$\begin{aligned} \bar{u}_{i,j}(\xi, t) &= \sum_{j=1}^n q_{i,j}(t) \eta_j(\xi), \\ \bar{w}_i^x(\xi, t) &= (1 - \xi) e_i^x(t) + \sum_{j=1}^n p_{i,j}^x(t) \eta_j(\xi), \\ \bar{w}_i^z(\xi, t) &= (1 - \xi) e_i^z(t) + \sum_{j=1}^n p_{i,j}^z(t) \eta_j(\xi), \\ \bar{\theta}_i(\xi, t) &= \sum_{j=1}^n \varphi_{i,j}(t) \eta_j(\xi), \end{aligned} \tag{13}$$

where  $q_{i,j}(t)$ ,  $p_{i,j}^x(t)$ ,  $p_{i,j}^z(t)$  and  $\varphi_{i,j}(t)$  are the generalized coordinates,  $\eta_j(\xi)$  are the corresponding trial functions, and  $n$  is the number of included modes. Because the bending stiffness of the cable is neglected, the cable model in this paper will be a string (wave)-like model. The platform is suspended freely in the shaft, which means that the suspension cable has a free end (in all three directions). So, the eigenfunctions of a fixed-free string with unit length are used as trial functions for the approximation in all three directions. The trial function for the model shown in Fig. 2 is

$$\eta_i(\xi) = \sqrt{2} \sin\left(\frac{2i-1}{2} \pi \xi\right). \tag{14}$$

Let

$$\mathbf{r} = [\mathbf{h}_1^T \quad \mathbf{h}_2^T \quad \mathbf{h}_3^T \quad \mathbf{h}_4^T \quad \mathbf{q}_p^T]^T, \tag{15}$$

where  $\mathbf{h}_i = [\mathbf{q}_i^T \quad (\mathbf{p}_i^x)^T \quad (\mathbf{p}_i^z)^T \quad \varphi_i^T]^T$  are the generalized coordinates of cable  $i$  and  $\mathbf{q}_p = [w_p^x \quad u_p \quad w_p^z \quad \theta_p^x \quad \theta_p^y \quad \theta_p^z]^T$  are the generalized coordinates of the platform. By using the Eqs. (11)–(15) and by substituting the Eqs. (4), (8) and (10) into the Lagrange's equation with constraints (see also [29])

$$\frac{d}{dt} \left( \frac{\partial L}{\partial \dot{\mathbf{r}}_j} \right) - \frac{\partial L}{\partial \mathbf{r}_j} = Q_j + \sum_{i=1}^n \lambda_i \frac{\partial \psi_i}{\partial \mathbf{r}_j}, \tag{16}$$

we obtain the following equations of motion for the platform system

$$\mathbf{M}\ddot{\mathbf{r}} + \mathbf{C}\dot{\mathbf{r}} + \mathbf{K}\mathbf{r} + (\boldsymbol{\psi}_r^b)^T \boldsymbol{\lambda}^b = \mathbf{f} + (\boldsymbol{\psi}_r^u)^T \boldsymbol{\lambda}^u, \tag{17}$$

$$\boldsymbol{\psi}^b(\mathbf{r}) = \mathbf{0}, \tag{18}$$

$$\boldsymbol{\psi}^u(\mathbf{r}) \perp \boldsymbol{\lambda}^u, \quad \boldsymbol{\psi}^u(\mathbf{r}) \geq \mathbf{0}, \quad \boldsymbol{\lambda}^u \geq \mathbf{0}, \tag{19}$$

where

- $\mathbf{M}$ ,  $\mathbf{C}$  and  $\mathbf{K}$  are the mass, damping and stiffness matrices;
- $\mathbf{f}$  is the generalized force vector. The entries of the matrices and force vector can be found in Appendix A.
- $\boldsymbol{\psi}_r^b = \partial \boldsymbol{\psi}^b / \partial \mathbf{r}$  is the Jacobian of the lateral and torsional constraint equations;
- $\boldsymbol{\psi}_r^u = \partial \boldsymbol{\psi}^u / \partial \mathbf{r}$  is the Jacobian of the longitudinal constraint equations;
- $\boldsymbol{\lambda}^b$  and  $\boldsymbol{\lambda}^u$  are the vector-valued Lagrangian multipliers, which are also the corresponding constraint forces.

The complementary condition in Eq. (19) can also be expressed as  $\boldsymbol{\psi}^u(\mathbf{r}) \cdot \boldsymbol{\lambda}^u = \mathbf{0}$  with both  $\boldsymbol{\psi}^u(\mathbf{r})$  and  $\boldsymbol{\lambda}^u$  being non-negative.

### 3. Numerical solution

#### 3.1. Equation of motion at the velocity level

In this section, a non-smooth generalized- $\alpha$  algorithm [25] will be used to solve the derived equations of motion. Firstly, by multiplying Eq. (17) with the Lebesgue measure  $dt$ , it can be rewritten at velocity level in the following form:

$$\mathbf{M}\dot{\mathbf{R}}dt + (\boldsymbol{\psi}_r^b)^T \boldsymbol{\lambda}^b dt = \mathbf{F}(\mathbf{r}, \mathbf{R}, t)dt + (\boldsymbol{\psi}_r^u)^T \boldsymbol{\lambda}^u dt, \tag{20}$$

where  $\mathbf{R} = \dot{\mathbf{r}}$ ,  $\mathbf{F}(\mathbf{r}, \mathbf{R}, t) = \mathbf{f} - \mathbf{C}\mathbf{R} - \mathbf{K}\mathbf{r}$ , or more briefly

$$\mathbf{M}d\mathbf{R} + (\boldsymbol{\psi}_r^b)^T d\mathbf{i}^b = \mathbf{F}(\mathbf{r}, \mathbf{R}, t)dt + (\boldsymbol{\psi}_r^u)^T d\mathbf{i}^u, \tag{21}$$

in which  $d\mathbf{i}^b$  and  $d\mathbf{i}^u$  are the impulse measure of the corresponding constraint forces.

As for the constraint equations, in most researches on multibody contact problems, these equations are expressed at velocity level in the form expressed in Eq. (22) by using the Newton impact law:

$$\text{if } \boldsymbol{\psi}^u(\mathbf{q}) \leq \mathbf{0} \text{ then } \mathbf{0} \leq \boldsymbol{\psi}_r^u \mathbf{R}(t^+) + e \boldsymbol{\psi}_r^u \mathbf{R}(t^-) \perp d\mathbf{i}^u \geq \mathbf{0}, \tag{22}$$

where the term  $\boldsymbol{\psi}^u(\mathbf{q}) \leq \mathbf{0}$  indicates that there is a collision between two objects,  $e$  is the coefficient of restitution,  $\mathbf{R}(t^-)$  and  $\mathbf{R}(t^+)$  are the velocities before and after the collision, respectively, and  $d\mathbf{i}^u$  is the impulse measure of the contact reactions. In the cable case, when  $\boldsymbol{\psi}^u(\mathbf{q}) \leq \mathbf{0}$ , cable is tensioned and moves together with the platform. So, the velocity after “collision” is 0, which means  $e$  in this case is 0. Since the constraint equations in this case contain both time-implicit terms and time-explicit terms, their time-differentiation can be obtained and expressed as

$$\frac{d\boldsymbol{\psi}}{dt} = \boldsymbol{\psi}_r \dot{\mathbf{r}} + \frac{\partial \boldsymbol{\psi}}{\partial t}. \tag{23}$$

Then, the Eqs. (18) and (19) can be rewritten at the velocity level and can be expressed as

$$\boldsymbol{\psi}_r^b \mathbf{R} + \partial \boldsymbol{\psi}^b / \partial t = \mathbf{0}, \tag{24}$$

$$\text{if } \boldsymbol{\psi}^u(\mathbf{q}) \leq \mathbf{0} \text{ then } (\boldsymbol{\psi}_r^u \mathbf{R} + \partial \boldsymbol{\psi}_r^u / \partial t) \perp d\mathbf{i}^u, \quad (\boldsymbol{\psi}_r^u \mathbf{R} + \partial \boldsymbol{\psi}_r^u / \partial t) \geq \mathbf{0}, \quad d\mathbf{i}^u \geq \mathbf{0}. \tag{25}$$

### 3.2. Time integration by the non-smooth generalized- $\alpha$ method

In order to solve the equations numerically (following the solving procedure as given in [25]), we firstly separate the contribution of the constraint forces from the contribution of the smooth forces such that

$$d\mathbf{R} = \dot{\mathbf{R}} dt + d\mathbf{w}, \tag{26}$$

with

$$\mathbf{M} \dot{\mathbf{R}} = \mathbf{F}, \tag{27}$$

$$\mathbf{M} d\mathbf{w} + (\boldsymbol{\psi}_r^b)^T d\mathbf{i}^b = (\boldsymbol{\psi}_r^u)^T d\mathbf{i}^u. \tag{28}$$

Secondly, defining the set  $\mathbf{A}$  as the active constraint of  $\boldsymbol{\psi}^u$  satisfying  $\boldsymbol{\psi}^u = 0$ , and  $\boldsymbol{\lambda}^A$  as the corresponding Lagrangian multiplier, and with the initial values at time  $t_N$  given by  $\mathbf{R}(t_N) = \bar{\mathbf{R}}(t_N)$ , where  $N$  indicates the  $N$ -th time step, the discretized form of the equations of motion of the system can be expressed in the following form by integrating Eq. (28) over a small finite time interval  $\Delta t = t_{N+1} - t_N$

$$\mathbf{M} \dot{\bar{\mathbf{R}}}_{N+1} = \mathbf{F}_{N+1}, \tag{29}$$

$$\mathbf{M}_{N+1} \mathbf{W}_{N+1} + (\boldsymbol{\psi}_{r,N+1}^b)^T \boldsymbol{\lambda}_{N+1}^b = (\boldsymbol{\psi}_{r,N+1}^A)^T \boldsymbol{\lambda}_{N+1}^A, \tag{30}$$

$$\boldsymbol{\psi}_{r,N+1}^b \mathbf{R}_{N+1} + \partial \boldsymbol{\psi}_{N+1}^b / \partial t = \mathbf{0}, \tag{31}$$

$$(\boldsymbol{\psi}_{r,N+1}^A \mathbf{R}_{N+1} + \partial \boldsymbol{\psi}_{r,N+1}^A / \partial t) \perp \boldsymbol{\lambda}_{N+1}^A, \quad \boldsymbol{\psi}_{r,N+1}^A \mathbf{R}_{N+1} + \partial \boldsymbol{\psi}_{r,N+1}^A / \partial t \geq \mathbf{0}, \quad \boldsymbol{\lambda}_{N+1}^A \geq \mathbf{0}, \tag{32}$$

Finally, following the non-smooth generalized- $\alpha$  method, the difference equations will be given by

$$\bar{\mathbf{r}}_{N+1} = \mathbf{r}_N + h\mathbf{R}_N + h^2(1/2 - \beta)\mathbf{a}_N + h^2\beta\mathbf{a}_{N+1}, \tag{33}$$

$$\bar{\mathbf{R}}_{N+1} = \mathbf{R}_N + h(1 - \gamma)\mathbf{a}_N + h\gamma\beta\mathbf{a}_{N+1}, \tag{34}$$

$$(1 - \alpha_m)\mathbf{a}_{N+1} + \alpha_m\mathbf{a}_N = (1 - \alpha_f)\dot{\bar{\mathbf{R}}}_{N+1} + \alpha_f(1 - \gamma)\dot{\bar{\mathbf{R}}}_N, \tag{35}$$

$$\mathbf{R}_{N+1} = \bar{\mathbf{R}}_{N+1} + \mathbf{W}_{N+1}, \tag{36}$$

$$\mathbf{r}_{N+1} = \bar{\mathbf{r}}_{N+1} + \frac{1}{2}h\mathbf{W}_{N+1}, \tag{37}$$

where  $\bar{\mathbf{r}}$  and  $\bar{\mathbf{R}}$  are the variables related to the smooth positions and velocities respectively, and where  $\mathbf{a}$  is an acceleration-like variable and  $h$  is the time step size. The parameters for the generalized- $\alpha$  method are defined as in [30]:

$$\alpha_m = \frac{2\rho_\infty - 1}{\rho_\infty + 1}, \quad \alpha_f = \frac{\rho_\infty}{\rho_\infty + 1}, \quad \gamma = \frac{1}{2} + \alpha_f - \alpha_m, \quad \beta = \frac{1}{4} \left( \gamma + \frac{1}{2} \right)^2, \tag{38}$$



where  $\rho_\infty = 0.8$  in this paper. Treating  $\bar{\mathbf{R}}, \mathbf{R}$  and  $\lambda^b$  as the sets of unknowns, the equations for the Newton iterations become:

$$\mathbf{S}_t \Delta \mathbf{x} = -\mathbf{res} + \mathbf{b}(\lambda_{N+1}^A - \lambda_{N+1}^{A*}), \tag{39}$$

where

$$\mathbf{S}_t = \begin{bmatrix} \gamma_t \mathbf{M}^* + \beta_t \mathbf{K}^* & \mathbf{C}^* + 1/2h\mathbf{K}^* & \mathbf{0} \\ -\mathbf{M}^* + \beta_t \mathbf{K}_t^{con*} & \mathbf{M}^* + 1/2h\mathbf{K}_t^{con*} & (\boldsymbol{\psi}_r^{b*})^T \\ \beta_t \boldsymbol{\psi}_{r2}^{b*} & \boldsymbol{\psi}_r^{b*} + 1/2h\boldsymbol{\psi}_{r2}^{b*} & \mathbf{0} \end{bmatrix}, \quad \Delta \mathbf{x} = \begin{bmatrix} \Delta \bar{\mathbf{R}} \\ \Delta \mathbf{R} \\ \Delta \lambda^b \end{bmatrix}, \tag{40}$$

$$\mathbf{res} = \begin{bmatrix} \mathbf{M}_{N+1}^* \dot{\bar{\mathbf{R}}}_{N+1}^* - \mathbf{F}_{N+1}^* \\ \mathbf{M}_{N+1}^* \mathbf{W}_{N+1}^* + (\boldsymbol{\psi}_q^{b*})^T \lambda_{N+1}^{b*} - (\boldsymbol{\psi}_q^{u*})^T \lambda_{N+1}^{A*} \\ \boldsymbol{\psi}_r^{b*} \mathbf{R}_{N+1}^* + \partial \boldsymbol{\psi}^{b*} / \partial t \end{bmatrix}, \quad \mathbf{b} = \begin{bmatrix} \mathbf{0} \\ (\boldsymbol{\psi}_r^{A*})^T \\ \mathbf{0} \end{bmatrix}, \tag{41}$$

in which

- $\gamma_t = (1 - \alpha_m) / [(1 - \alpha_f)\gamma h]$  and  $\beta_t = \beta h / \gamma - 1/2h$ , the superscript \* denotes the value of a variable at the  $k$ th Newton iteration;
- $\mathbf{K}_t^{con} = \partial(\mathbf{M}\mathbf{W} + (\boldsymbol{\psi}_q^b)^T \lambda^b - (\boldsymbol{\psi}_q^u)^T \lambda^A) / \partial \mathbf{r}$ ;
- $\boldsymbol{\psi}_{r2}^b = \partial(\boldsymbol{\psi}_{r,N+1}^b \mathbf{R}_{N+1}) / \partial \mathbf{r}_{N+1}$

The complementary condition can also be linearized as

$$\mathbf{0} \leq \boldsymbol{\psi}_r^A \mathbf{R} + \partial \boldsymbol{\psi}_r^A / \partial t + \mathbf{c} \Delta \mathbf{x}, \tag{42}$$

where

$$\mathbf{c} = [\beta_t \boldsymbol{\psi}_{r2,N+1}^{A*} \quad \boldsymbol{\psi}_{r,N+1}^{A*} + 1/2h\boldsymbol{\psi}_{r2,N+1}^{A*} \quad \mathbf{0}], \tag{43}$$

in which  $\boldsymbol{\psi}_{r2,N+1}^{A*} = \partial(\boldsymbol{\psi}_{r,N+1}^A \mathbf{R}_{N+1} + \partial \boldsymbol{\psi}_{r,N+1}^A / \partial t) / \partial \mathbf{r}_{N+1}$ . By substituting Eq. (39) into Eq. (43), one can derive the standard form of the linear complimentary problem (LCP):

$$(\bar{\mathbf{M}} \boldsymbol{\Lambda}_{n+1}^A + \bar{\mathbf{f}}) \perp \boldsymbol{\Lambda}_{n+1}^A, \quad \bar{\mathbf{M}} \boldsymbol{\Lambda}_{n+1}^A + \bar{\mathbf{f}} \geq \mathbf{0}, \quad \boldsymbol{\Lambda}_{n+1}^A \geq \mathbf{0}, \tag{44}$$

with

$$\begin{cases} \bar{\mathbf{M}} = \mathbf{c} \mathbf{S}_t^{-1} \mathbf{b}, \\ \bar{\mathbf{f}} = \boldsymbol{\psi}_{r,N+1}^{A*} \mathbf{R}_{N+1}^* - \mathbf{c} \mathbf{S}_t^{-1} \mathbf{res} - \mathbf{c} \mathbf{S}_t^{-1} \mathbf{b} \boldsymbol{\Lambda}_{N+1}^{A*} + \partial \boldsymbol{\psi}_r^A / \partial t. \end{cases} \tag{45}$$

$\boldsymbol{\Lambda}_{N+1}^A$  can then be obtained by solving this LCP based on Lemke's algorithm [23]. This solving procedure by the non-smooth generalized- $\alpha$  method is given in detail in Appendix B.

### 3.3. ADAMS simulation

ADAMS simulation is an alternative way in investigating the non-smooth dynamics of the multi-cable suspension system. Based on the finite element modelling method, each cable is discretized into finite rigid cylinder elements with the same length (1 m in this paper), as shown in Fig. 3. Adjacent cylinders of the same cable are connected by the *force field* which is a flexible connecting procedure provided by ADAMS, which also contains all the mechanical parameters, especially the longitudinal-torsional stiffness of the cable. All the cables are connected to the platform by the spherical joint and each cable is connected to its corresponding winch by fixed joint. It should be noticed, that when the internal damping of the cable is set equal to zero, then the simulation may fail due to “unknown reasons” (may be the poor performance of the ADAMS's numerical algorithm when dealing with systems with quantities of components and constraints). So, a small damping value is introduced to let the simulation work. The critical damping coefficient for the longitudinal vibration of a cable with unit length is  $2\sqrt{\rho Q_1/L} = 4.65 \times 10^4$ , while in our model and in the ADAMS simulation, the damping coefficient is 20 in longitudinal vibration and 2 in both lateral and torsional vibrations. In the numerical simulation, the damping is introduced by using the Rayleigh's dissipation function. However, the damping coefficient we use in the paper is not a typical parameter for the hoisting cables (which should be obtained by accurate experiments), it is only used for letting the ADAMS simulation run.

In order to model the releasing process of the cables, an accurate and time-saving simulation strategy is used here to carry out the simulation. The strategy can be summarized as follows (see also Fig. 4). Firstly, a base line is defined, and to each cylinder a displacement sensor is attached. Since the cylinders are fixed to the winch, they will follow the movement of their winch, and the *force field* will not work during this stage. When a sensor detects that the upper side of its cylinder reaches the base line, a subprogram will be activated to deactivate the fixed joint between this cylinder and its winch. After that, the *force field* is activated.

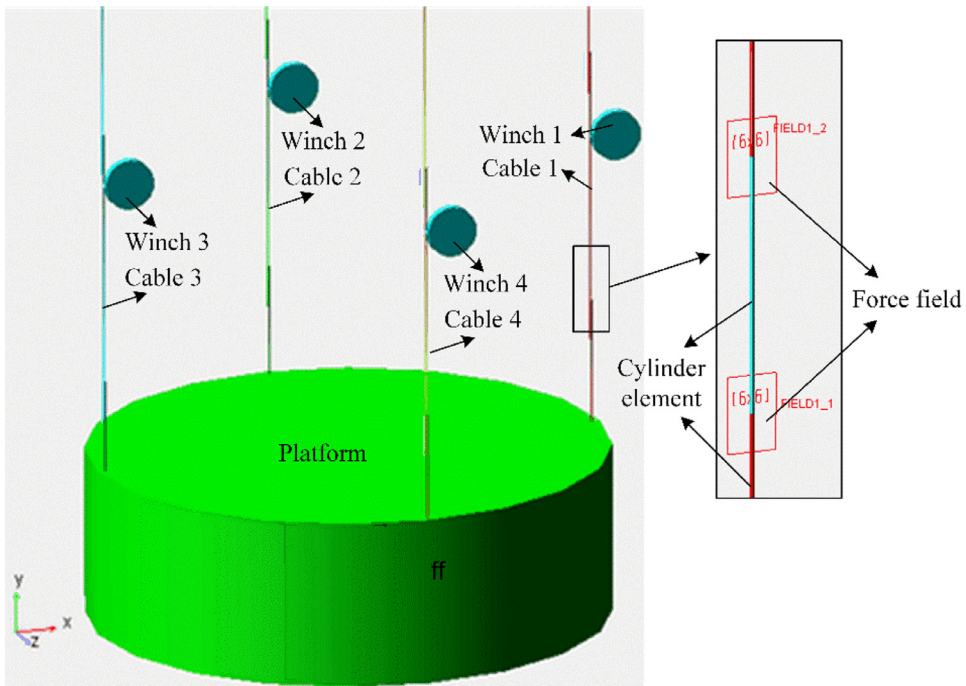


Fig. 3. ADAMS simulation model.

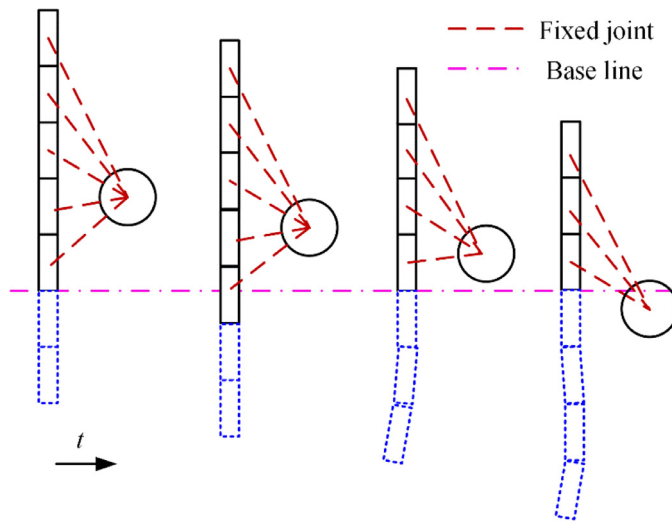


Fig. 4. Schematic of the ADAMS Driving Strategy.

**4. Numerical simulation**

The typical parameters for a multi-cable driven parallel suspension platform system are as follows:  $\rho = 6 \text{ kg/m}$ ,  $J_c = 1.5 \times 10^{-4} \text{ kgm}$ ,  $Q_1 = 9 \times 10^7 \text{ N}$ ,  $Q_4 = 3 \times 10^3 \text{ Nm}^2$ ,  $Q_{23,1} = Q_{23,3} = 3 \times 10^5 \text{ Nm}$ ,  $Q_{23,2} = Q_{23,4} = -3 \times 10^5 \text{ Nm}$ ,  $m_p = 8000 \text{ kg}$ ,  $J_p^y = 3.6 \times 10^4 \text{ kgm}^2$ ,  $J_p^x = J_p^z = 3.8 \times 10^4 \text{ kgm}^2$ . The prescribed movement curves of the platform are shown in Fig. 5. In order to simulate the slack cable, the longitudinal excitations of cables are assumed in Eqs. (47) and (48), and the lateral excitation is given in Eq. (46).

$$e_1^z(t) = 0.02 \times \sin(\pi t), \tag{46}$$

$$e_3^y(t) = 0.1 \times \sin(2/15 \times \pi t), \tag{47}$$

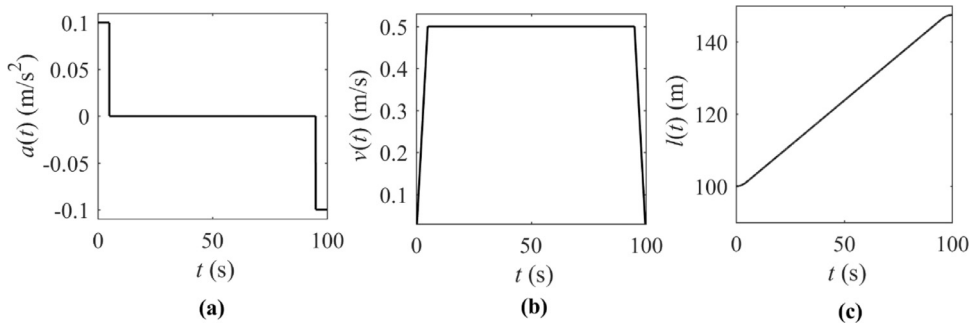


Fig. 5. Prescribed movement of the platform.

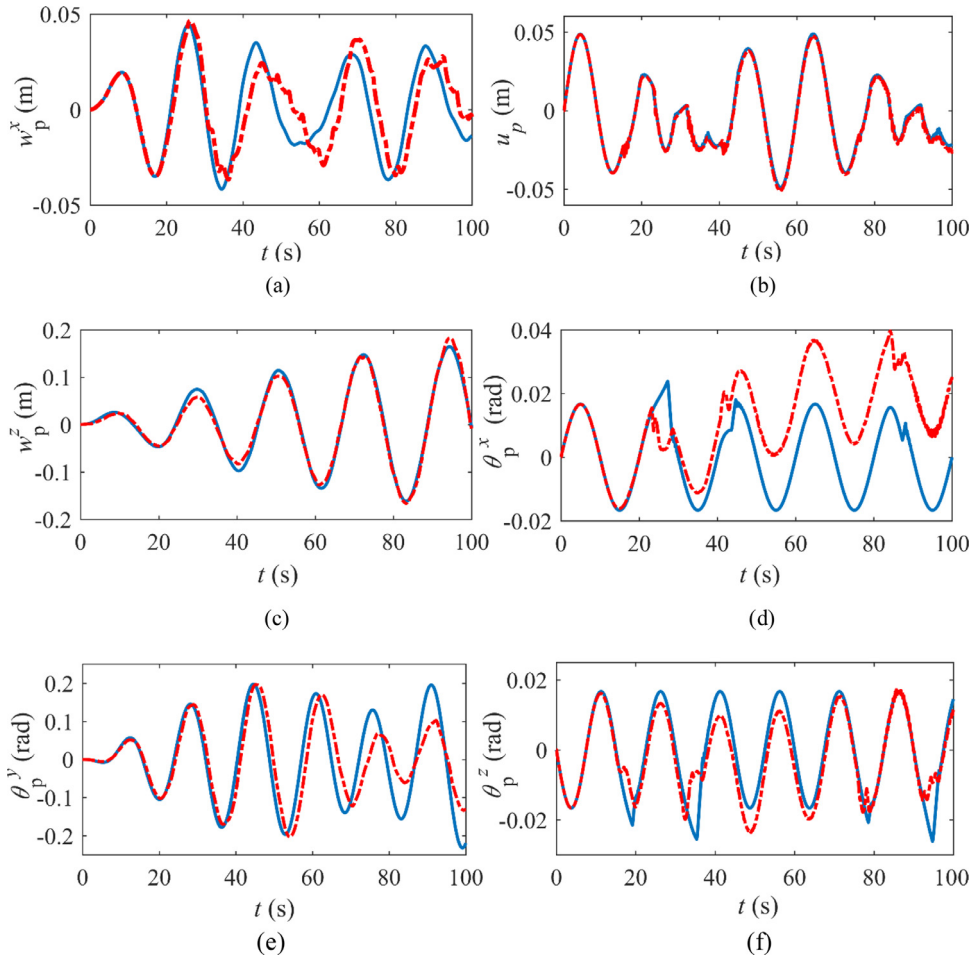


Fig. 6. Dynamical displacements of the platform versus time  $t$ : Non-smooth generalized- $\alpha$  method (solid line) and ADAMS simulation (dashed line).

$$e_4^y(t) = 0.1 \times \sin(0.1\pi t). \tag{48}$$

The numerical simulations are carried out with time step size  $\Delta t = 0.001$  s, and number of included modes  $n = 20$ . The results are shown in Figs. 6–8.

From Figs. 6–8, it can be seen that the numerical results agree well with the ADAMS simulations. It can also be observed in Fig. 7 that negative cable tension values occurred in the ADAMS simulations during some periods. This can be explained as follows. In the ADAMS simulation, the cable is discretised into finite rigid cylinders. The adjacent cylinders are connected by a force field, which works like springs, and contains all the cable stiffness parameters, so that it can act like a cable. By measuring the relative displacement between two adjacent cylinders, ADAMS can give the force relations between them,

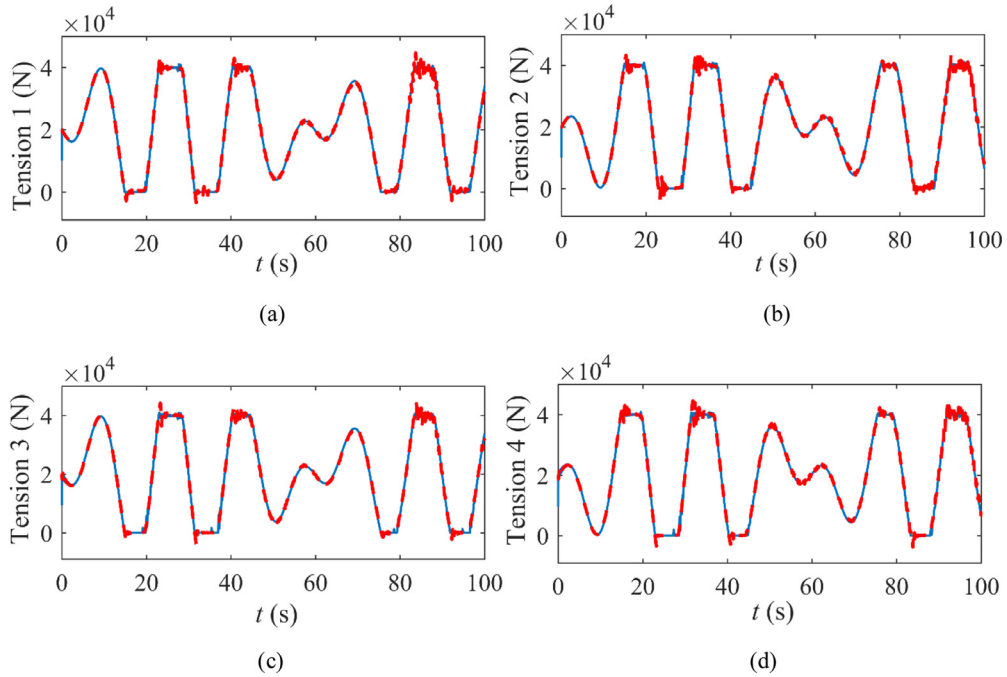


Fig. 7. Axial tension of the suspension cables versus time  $t$ : Non-smooth generalized- $\alpha$  method (solid line) and ADAMS simulation (dashed line).

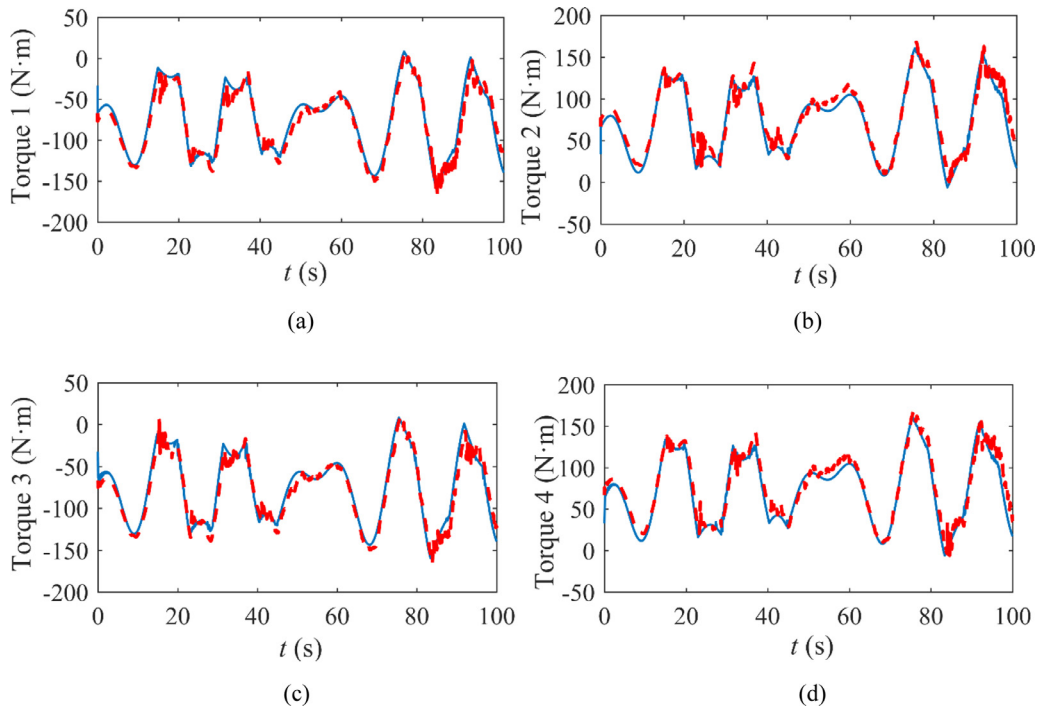


Fig. 8. Axial torque of the suspension cables versus time  $t$ : Non-smooth generalized- $\alpha$  method (solid line) and ADAMS simulation (dashed line).

which will be the tension, torque and bending moment of the cable. Thus, when the cable modelled in ADAMS is pushed, its tension will become negative before it bends, and this is also the main reason for the differences between the ADAMS simulation and the other two numerical results. For example, Fig. 7(b) has shown that there is a relatively large negative tension of cable 2 at around 22 s. This “pushing force” has greatly influenced the rotation of the platform about X- axis, so, a dent appeared in the ADAMS simulation result in Fig. 6(d) at around 22 s.

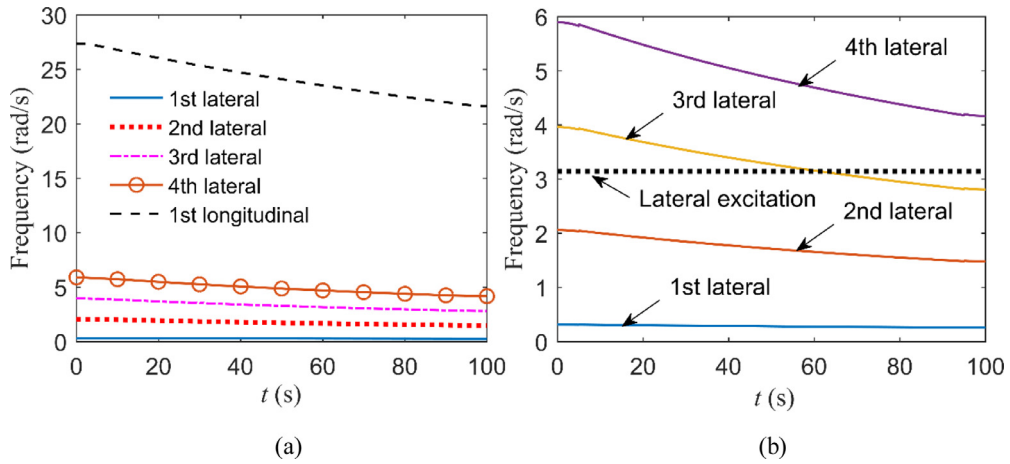


Fig. 9. The longitudinal and lateral natural frequency.

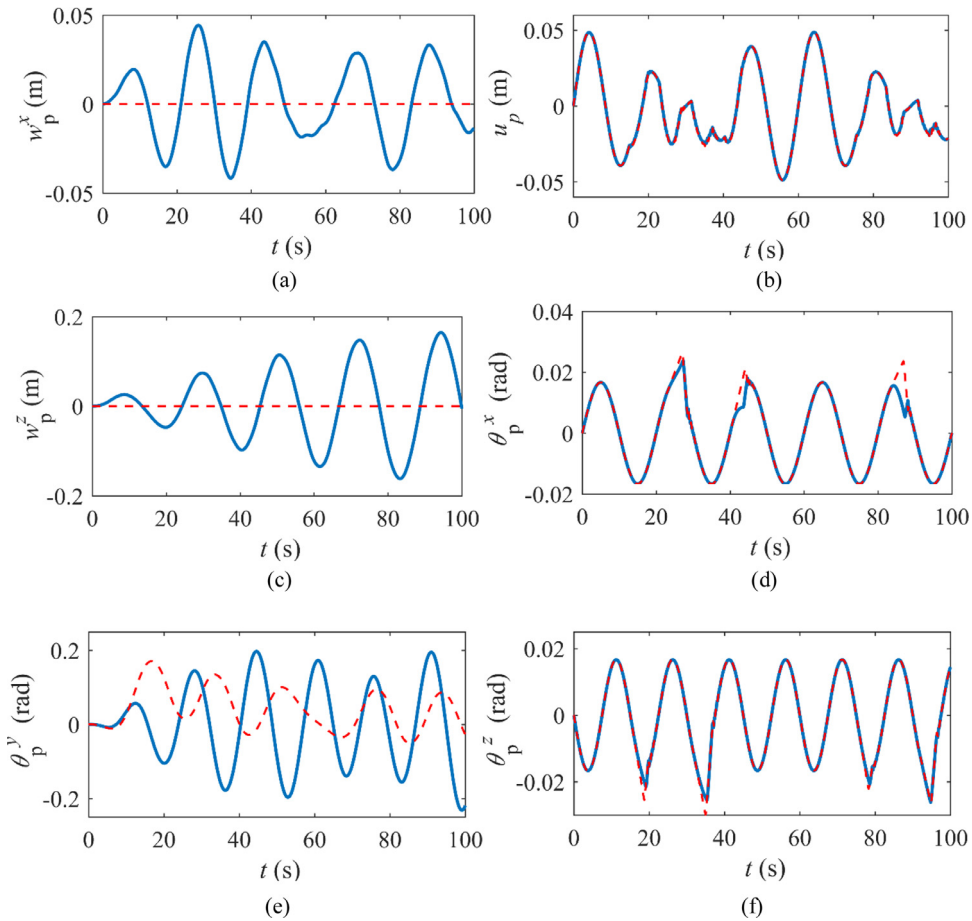


Fig. 10. Comparison of the platform dynamic displacements with (solid line) and without (dashed line) considering the lateral characters of the cables.

Fig. 6 shows the dynamic displacements of the platform. It can be seen that there are velocity jumps in y direction, which is caused by the non-smooth tension behaviour in the cables, as shown in Fig. 7. When the tension of a cable becomes 0 N, this cable will be slack. The state of the cables alters between slack and tensioned, this will introduce shocks to the system. Since the platform suspends all kinds of construction machines and also carries workers, those shocks may cause severe accidents. The maximal rotation of the platform around the y axis is about 0.2 rad, which is relatively small, however, since the radius of the platform is 3 m, the displacement of the edge of the platform will be a considerable 0.6 m, which is also

a potential risk to the objects on the platform. From Fig. 9(a), Eqs. (47) and (48), one can see that the first longitudinal natural frequency is always much larger than the longitudinal excitation frequencies, which are  $2\pi/15$  rad/s and  $0.1\pi$  rad/s, respectively. So, no resonance will occur even for a very long cable length (the first longitudinal natural frequency will be 5.23 rad/s when the cable length is 1000 m). As shown in Fig. 9(b), the lateral excitation in  $z$ -direction is  $\pi$  rad/s, which is always close or equal to the third lateral natural frequency of the system, and is also close to the second and fourth lateral frequency. So, the lateral vibration amplitude of the platform in  $z$ -direction is increasing throughout the simulation, as shown in Fig. 6(c). Fig. 8 shows that the torque of a cable is mainly caused by its axial tension.

In most research work on this subject [2,20–22] the lateral properties of the cable are not taken into account. Fig. 10 shows the dynamic responses of the platform obtained by the non-smooth generalized- $\alpha$  method with and without considering the lateral properties of the cable, from which it can be seen that the lateral and torsional responses of the platform are inaccurate. This can be explained as follows: while the torsional displacement of the platform will induce the lateral vibrations of the cables, the lateral movement of the cables will in turn affect the rotation of the platform. Thus, it is essential to include the lateral properties of the cables to accurately simulate their dynamic responses.

### 5. Conclusions

The equations of motion for a multi-cable driven parallel suspension platform system are derived using Lagrange's principle with constraints. The longitudinal, in-plane and out-of-plane lateral, torsional and longitudinal-torsional coupled dynamic behaviours of the suspension cables, and the dynamic behaviours of the platform in all directions are included, as well as the slackness property of the cables.

A non-smooth generalized- $\alpha$  method is applied to obtain numerically the non-smooth dynamic responses of the system. The results are in good agreement with an ADAMS simulation. The numerical results clearly indicate that a change in tension in the suspension cables may lead to dynamic velocity jumps of the platform in  $y$ -direction, which may cause severe accidents. The rotation of the platform about the  $Y$ -axis may also lead to additional and significant forces acting on the objects on the platform that are suspended close to the edge of the platform.

The lateral properties of the cables have a great effect on the dynamic responses of the system investigated in this paper. So, controlling the lateral vibrations of the cables is an essential part in achieving a steady movement of the platform. For the dynamical modelling of the multi-cable driven manipulators, it is recommended to include the mass, longitudinal, torsional, in-plane and out-of-plane lateral and longitudinal-torsional properties of the cables, so as to achieve accurate modelling results. Experiments on accurately obtaining those cable parameters (including damping) are also very important, as well as a better understanding of the numerical algorithm damping.

### Acknowledgements

This work is supported by the National Key Research and Development Program (2016YFC0600901) and the National Natural Science Foundation of China (51475456). The first and second author also thank the China Scholarship Council for providing a scholarship to perform the research as presented in this paper at the Delft Institute of Applied Mathematics of the Delft University of Technology.

### Appendix A

The entries of the matrices and force vector in Eq. (17) are defined as follows:

$$\mathbf{M} = \text{diag}(\mathbf{M}_1^c \quad \mathbf{M}_2^c \quad \mathbf{M}_3^c \quad \mathbf{M}_4^c \quad \mathbf{M}_p), \tag{A.1}$$

$$\mathbf{C} = \text{diag}(\mathbf{C}_1^c \quad \mathbf{C}_2^c \quad \mathbf{C}_3^c \quad \mathbf{C}_4^c \quad \mathbf{C}_p), \tag{A.2}$$

$$\mathbf{K} = \text{diag}(\mathbf{K}_1^c \quad \mathbf{K}_2^c \quad \mathbf{K}_3^c \quad \mathbf{K}_4^c \quad \mathbf{K}_p), \tag{A.3}$$

$$\mathbf{Q} = \left[ (\mathbf{Q}_1^c)^T \quad (\mathbf{Q}_2^c)^T \quad (\mathbf{Q}_3^c)^T \quad (\mathbf{Q}_4^c)^T \quad (\mathbf{Q}_p)^T \right]^T, \tag{A.4}$$

where

$$\mathbf{M}_i^c = \text{diag}(\mathbf{M}_i^L \quad \mathbf{M}_i^\varphi \quad \mathbf{M}_i^x \quad \mathbf{M}_i^z), \tag{A.5}$$

$$\mathbf{C}_i^c = \text{diag}(\mathbf{C}_i^L \quad \mathbf{C}_i^\varphi \quad \mathbf{C}_i^x \quad \mathbf{C}_i^z), \tag{A.6}$$

$$\mathbf{K}_i^c = \begin{bmatrix} \mathbf{K}_i^L & \mathbf{K}_i^{L\varphi} & \mathbf{0} \\ \mathbf{K}_i^{L\varphi} & \mathbf{K}_i^\varphi & \mathbf{0} \\ \mathbf{0} & \mathbf{0} & \mathbf{K}_i^x \\ \mathbf{0} & \mathbf{0} & \mathbf{0} & \mathbf{K}_i^z \end{bmatrix}, \tag{A.7}$$

$$\mathbf{Q}_i^c = \left[ (\mathbf{Q}_i^l)^T \quad (\mathbf{Q}_i^\varphi)^T \quad (\mathbf{Q}_i^x)^T \quad (\mathbf{Q}_i^z)^T \right]^T, \tag{A.8}$$

$$\mathbf{M}_p = \text{diag}(m_p \quad m_p \quad m_p \quad J_p^x \quad J_p^y \quad J_p^z), \tag{A.9}$$

$$\mathbf{C}_p = \mathbf{0}, \quad \mathbf{K}_p = \mathbf{0}, \tag{A.10}$$

$$\mathbf{Q}_p = [0 \quad m_p(g - a(t)) \quad 0 \quad 0 \quad 0 \quad 0]^T, \tag{A.11}$$

in which

$$\mathbf{M}_{i,kj}^l = \rho l_i(t) \int_0^1 \eta_j \eta_k d\xi, \tag{A.12}$$

$$\mathbf{M}_{i,kj}^\varphi = J_c l_i(t) \int_0^1 \eta_j \eta_k d\xi, \tag{A.13}$$

$$\mathbf{M}_{i,kj}^x = \mathbf{M}_{i,kj}^z = \rho l_i(t) \int_0^1 \eta_j \eta_k d\xi, \tag{A.14}$$

$$\begin{aligned} \mathbf{C}_{i,kj}^l &= \rho v_i(t) \int_0^1 \eta_j(\xi) \eta_k(\xi) d\xi + \rho v_i(t) \int_0^1 (1 - \xi) \eta'_j(\xi) \eta_k(\xi) d\xi + \dots \\ &\quad - \rho v_i(t) \int_0^1 (1 - \xi) \eta_j(\xi) \eta'_k(\xi) d\xi, \end{aligned} \tag{A.15}$$

$$\begin{aligned} \mathbf{C}_{i,kj}^\varphi &= J_c v_i(t) \int_0^1 \eta_j(\xi) \eta_k(\xi) d\xi + J_c v_i(t) \int_0^1 (1 - \xi) \eta'_j(\xi) \eta_k(\xi) d\xi + \dots \\ &\quad - J_c v_i(t) \int_0^1 (1 - \xi) \eta_j(\xi) \eta'_k(\xi) d\xi, \end{aligned} \tag{A.16}$$

$$\begin{aligned} \mathbf{C}_{i,kj}^x &= \mathbf{C}_{i,kj}^z = \rho v_i(t) \int_0^1 \eta_j(\xi) \eta_k(\xi) d\xi + \rho v_i(t) \int_0^1 (1 - \xi) \eta'_j(\xi) \eta_k(\xi) d\xi + \dots \\ &\quad - \rho v_i(t) \int_0^1 (1 - \xi) \eta_j(\xi) \eta'_k(\xi) d\xi, \end{aligned} \tag{A.17}$$

$$\begin{aligned} \mathbf{K}_{i,kj}^l &= \frac{Q_1}{l_i(t)} \int_0^1 \eta'_j(\xi) \eta'_k(\xi) d\xi + \frac{\rho v_i^2(t)}{l_i(t)} \int_0^1 \xi \eta'_j(\xi) \eta_k(\xi) d\xi + \dots \\ &\quad \rho a_i(t) \int_0^1 (1 - \xi) \eta'_j(\xi) \eta_k(\xi) d\xi - \frac{\rho v_i^2(t)}{l_i(t)} \int_0^1 (1 - \xi)^2 \eta'_j(\xi) \eta'_k(\xi) d\xi, \end{aligned} \tag{A.18}$$

$$\begin{aligned} \mathbf{K}_{i,kj}^\varphi &= \frac{Q_4}{l_i(t)} \int_0^1 \eta'_j(\xi) \eta'_k(\xi) d\xi + \frac{J v_i^2(t)}{l_i(t)} \int_0^1 \xi \eta'_j(\xi) \eta_k(\xi) d\xi + \dots \\ &\quad \times J a_i(t) \int_0^1 (1 - \xi) \eta'_j(\xi) \eta_k(\xi) d\xi - \frac{J v_i^2(t)}{l_i(t)} \int_0^1 (1 - \xi)^2 \eta'_j(\xi) \eta'_k(\xi) d\xi, \end{aligned} \tag{A.19}$$

$$\mathbf{K}_{i,kj}^{L\varphi} = \int_0^1 \frac{Q_{23,i}}{l_i(t)} \eta'_j(\xi) \eta'_k(\xi) d\xi, \quad \mathbf{K}_{i,kj}^{\varphi L} = \int_0^1 \frac{Q_{23,i}}{l_i(t)} \eta'_j(\xi) \eta'_k(\xi) d\xi, \tag{A.20}$$

$$\begin{aligned} \mathbf{K}_{i,kj}^x &= \mathbf{K}_{i,kj}^z = \int_0^1 \rho a_i(t) (1 - \xi) \eta'_j(\xi) \eta_k(\xi) d\xi - \int_0^1 \frac{\rho v_i^2(t)}{l_i(t)} (1 - \xi)^2 \eta'_j(\xi) \eta'_k(\xi) d\xi + \dots \\ &\quad \times \int_0^1 \frac{m(g - a_i)}{4l_i} \eta'_j(\xi) \eta'_k(\xi) d\xi + \int_0^1 \rho (g - a_i(t)) (1 - \xi) \eta'_j(\xi) \eta'_k(\xi) d\xi + \dots \int_0^1 \frac{\rho v_i^2(t)}{l_i(t)} \xi \eta'_j(\xi) \eta'_k(\xi) d\xi, \end{aligned} \tag{A.21}$$

$$\mathbf{Q}_{i,k}^l = - \int_0^1 \rho(l_i(t)a_i(t) + v_i^2(t) - l_i(t)g)\eta_k(\xi)d\xi + \dots - \int_0^1 (\rho gl_i(t) - \rho v_i^2(t))(1 - \xi)\eta'_k(\xi)d\xi - \int_0^1 \frac{1}{4}mg\eta'_k(\xi)d\xi, \tag{A.22}$$

$$\mathbf{Q}_{i,j}^\varphi = -mg\frac{Q_{2,i}}{Q_{1,i}}\int_0^1 \eta'_k(\xi)d\xi - \rho l_i(t)g\frac{Q_{2,i}}{Q_{1,i}}\int_0^1 (1 - \xi)\eta'_k(\xi)d\xi, \tag{A.23}$$

$$\begin{aligned} \mathbf{Q}_{i,k}^x &= \int_0^1 \rho v_i(t) \left( \dot{e}_i^x(t) - \frac{v_i(t)}{l_i(t)} e_i^x(t) \right) (1 - \xi)^2 \eta'_k(\xi) d\xi + \dots \\ &\times \int_0^1 \frac{\rho v_i^2(t)}{l_i(t)} e_i^x(t) \xi (1 - \xi) \eta'_k(\xi) d\xi + \dots \\ &\times \int_0^1 \rho (g - a_i(t)) e_i^x(t) (1 - \xi) \eta'_k(\xi) d\xi + \dots \\ &\times \int_0^1 \rho (a_i(t) e_i^x(t) - l_i(t) \ddot{e}_i^x(t)) (1 - \xi) \eta_k(\xi) d\xi + \dots \\ &\times \int_0^1 \rho \left( \frac{2v_i^2(t)}{l_i(t)} e_i^x(t) - a_i(t) e_i^x(t) - 2v_i(t) \dot{e}_i^x(t) \right) \xi \eta_k(\xi) d\xi + \dots \\ &\times \int_0^1 \frac{m(g - a_i(t))}{l_i(t)} e_i^x(t) \eta'_k(\xi) d\xi, \end{aligned} \tag{A.24}$$

$$\begin{aligned} \mathbf{Q}_{i,k}^z &= \int_0^1 \rho v_i(t) \left( \dot{e}_i^z(t) - \frac{v_i(t)}{l_i(t)} e_i^z(t) \right) (1 - \xi)^2 \eta'_k(\xi) d\xi + \dots \\ &\times \int_0^1 \frac{\rho v_i^2(t)}{l_i(t)} e_i^z(t) \xi (1 - \xi) \eta'_k(\xi) d\xi + \dots \\ &\times \int_0^1 \rho (g - a_i(t)) e_i^z(t) (1 - \xi) \eta'_k(\xi) d\xi + \dots \\ &\times \int_0^1 \rho (a_i(t) e_i^z(t) - l_i(t) \ddot{e}_i^z(t)) (1 - \xi) \eta_k(\xi) d\xi + \dots \\ &\times \int_0^1 \rho \left( \frac{2v_i^2(t)}{l_i(t)} e_i^z(t) - a_i(t) e_i^z(t) - 2v_i(t) \dot{e}_i^z(t) \right) \xi \eta_k(\xi) d\xi + \dots \\ &\times \int_0^1 \frac{m(g - a_i(t))}{l_i(t)} e_i^z(t) \eta'_k(\xi) d\xi. \end{aligned} \tag{A.25}$$

**Appendix B**

The solution procedure in the non-smooth generalized- $\alpha$  algorithm.

Function  $[\mathbf{r}_{N+1}, \mathbf{R}_{N+1}, \dot{\mathbf{R}}_{N+1}, \mathbf{a}_{N+1}] = \text{Non\_smooth\_alpha}(\mathbf{r}_N, \mathbf{R}_N, \dot{\mathbf{R}}_N, \mathbf{a}_N)$

```

 $\dot{\mathbf{R}}_{N+1} = \mathbf{0};$ 
 $\mathbf{a}_{N+1} = 1/(1 - \alpha_m)(\alpha_f \dot{\mathbf{R}}_N - \alpha_m \mathbf{a}_N);$ 
 $\dot{\mathbf{R}}_{N+1} = \mathbf{R}_N + h(1 - \gamma)\mathbf{a}_N + h\gamma\mathbf{a}_{N+1};$ 
 $\mathbf{R}_{N+1} = \dot{\mathbf{R}}_{N+1};$ 
 $\mathbf{r}_{N+1} = \mathbf{r}_N + h\mathbf{R}_N + h^2(1/2 - \beta)\mathbf{a}_N + h^2\beta\mathbf{a}_{N+1}$ 
 $\lambda_{N+1}^b = \mathbf{0};$ 
Define the active set as:  $\mathbf{A} = \{i | \psi_i^b \leq 0\};$ 
 $\lambda_{N+1}^A = \mathbf{0};$ 
for  $i = 1: i_{\max}$ 
  Compute res
  if  $\|\mathbf{res}\| \leq tol$ 
    break
  end if
   $\lambda_{N+1}^{A*} = \lambda_{N+1}^A;$ 
  Compute  $\mathbf{S}_i, \mathbf{b}, \mathbf{res}, \bar{\mathbf{M}}$  and  $\bar{\mathbf{f}};$ 
   $[\sim, \lambda_{N+1}^A] = \text{LCPSolver}(\bar{\mathbf{M}}, \bar{\mathbf{f}});$ 

```



$$\Delta \mathbf{x} = \mathbf{S}_t^{-1} [-\mathbf{res} + \mathbf{b}(\lambda_{N+1}^A - \lambda_{N+1}^{A*})];$$

$$\bar{\mathbf{R}}_{N+1} = \bar{\mathbf{R}}_{N+1} + \Delta \bar{\mathbf{R}};$$

$$\mathbf{R}_{N+1} = \mathbf{R}_{N+1} + \Delta \mathbf{R};$$

$$\mathbf{r}_{N+1} = \mathbf{r}_{N+1} + \beta_t \Delta \bar{\mathbf{R}} + 1/2 \cdot h \cdot \Delta \mathbf{R};$$

$$\dot{\bar{\mathbf{R}}}_{N+1} = \dot{\bar{\mathbf{R}}}_{N+1} + \gamma_t \Delta \bar{\mathbf{R}};$$

$$\lambda_{N+1}^b = \lambda_{N+1}^b + \Delta \lambda^b;$$

end for

$$\mathbf{a}_{N+1} = \mathbf{a}_{N+1} + (1 - \alpha_f)/(1 - \alpha_m) \dot{\bar{\mathbf{R}}}_{N+1};$$

$$\lambda^b = \lambda_{N+1}^b/h; \lambda^u = \lambda_{N+1}^u/h;$$

end function

## References

- [1] Y. Wang, G. Cao, N. Wang, W. Peng, Dynamic responses of cable-driven parallel sinking platform, *Math. Comput. Model. Dyn. Syst.* 23 (2017) 104–115.
- [2] X.G. Shao, Z.C. Zhu, Q.G. Wang, P.C.Y. Chen, B. Zi, G.H. Cao, Non-smooth dynamical analysis and experimental validation of the cable-suspended parallel manipulator, *Proc. Inst. Mech. Eng. Part C-J. Mech. Eng. Sci.* 226 (2012) 2456–2466.
- [3] Y. Zhang, S.K. Agrawal, P. Hagedorn, Modeling and control of flexible transporter system with arbitrarily time-varying cable lengths, in: *ASME 2003 Int. Des. Eng. Tech. Conf. Comput. Inf. Eng. Conf.*, 2003, pp. 2–6.
- [4] J. Wang, Y. Pi, Y. Hu, X. Gong, Modeling and dynamic behavior analysis of a coupled multi-cable double drum winding hoister with flexible guides, *Mech. Mach. Theory* 108 (2017) 191–208.
- [5] S. Kaczmarczyk, The passage through resonance in a catenary-vertical cable hoisting system with slowly varying length, *J. Sound Vib.* 208 (1997) 243–269.
- [6] S. Kaczmarczyk, W. Ostachowicz, Transient vibration phenomena in deep mine hoisting cables. Part 1: mathematical model, *J. Sound Vib.* 262 (2003) 219–244.
- [7] W.D. Zhu, J. Ni, Energetics and stability of translating media with an arbitrarily varying length, *J. Vib. Acoust.* 122 (2000) 295–304.
- [8] J. Wang, G. Cao, Z. Zhu, Y. Wang, W. Peng, Lateral response of cable-guided hoisting system with time-varying length: theoretical model and dynamics simulation verification, *Proc. Inst. Mech. Eng. Part C J. Mech. Eng. Sci.* 229 (2015) 2908–2920.
- [9] H. Ren, W.D. Zhu, An accurate spatial discretization and substructure method with application to moving elevator cable-car systems—part II: application, *J. Vib. Acoust.* 135 (2013) 51037.
- [10] J.L. Huang, W.D. Zhu, Nonlinear dynamics of a high-dimensional model of a rotating Euler–Bernoulli beam under the gravity load, *J. Appl. Mech.* 81 (2014) 101007.
- [11] W.D. Zhu, H. Ren, C. Xiao, A nonlinear model of a slack cable with bending stiffness and moving ends with application to elevator traveling and compensation cables, *J. Appl. Mech.* 78 (2011) 41017.
- [12] W. Fan, W.D. Zhu, H. Ren, A new singularity-free formulation of a three-dimensional Euler–Bernoulli beam using Euler parameters, *J. Comput. Nonlinear Dyn* 11 (2016) 41013.
- [13] W.D. Zhu, W. Fan, Y.G. Mao, G.X. Ren, Three-dimensional dynamic modeling and analysis of moving elevator traveling cables, *Proc. Inst. Mech. Eng. Part K J. Multi-Body Dyn.* 231 (2017) 167–180.
- [14] S.H. Sandilo, W.T. van Horssen, On variable length induced vibrations of a vertical string, *J. Sound Vib.* 333 (2014) 2432–2449.
- [15] S.H. Sandilo, W.T. van Horssen, On a cascade of autoresonances in an elevator cable system, *Nonlinear Dyn.* 80 (2015) 1613–1630.
- [16] N.V. Gaiko, W.T. van Horssen, On wave reflections and energetics for a semi-infinite traveling string with a nonclassical boundary support, *J. Sound Vib.* 370 (2016) 336–350.
- [17] T. Akkaya, W.T. van Horssen, On the transverse vibrations of strings and beams on semi-infinite domains, in: *Procedia IUTAM*, Elsevier, 2016, pp. 266–273.
- [18] W.T. van Horssen, On the influence of lateral vibrations of supports for an axially moving string, *J. Sound Vib.* 268 (2003) 323–330.
- [19] W.T. Van Horssen, S.V. Ponomareva, On the construction of the solution of an equation describing an axially moving string, *J. Sound Vib.* 287 (2005) 359–366.
- [20] B.L. Wang, J. Unger, J.D. Lee, Stiffness study of a parallel link robot crane for shipbuilding applications, *J. Offshore Mech. Arct. Eng.* 111 (1989) 183.
- [21] S. Kawamura, H. Kino, C. Won, High-speed manipulation by using parallel wire-driven robots, *Robotica* 18 (2000) 13–21.
- [22] B. Zi, B.Y. Duan, J.L. Du, H. Bao, Dynamic modeling and active control of a cable-suspended parallel robot, *Mechatronics* 18 (2008) 1–12.
- [23] C.E. Lemke, J.T. Howson Jr, Equilibrium points of bimatrix games, *J. Soc. Ind. Appl. Math.* 12 (1964) 413–423.
- [24] F. Pfeiffer, M. Foerg, H. Ulbrich, Numerical aspects of non-smooth multibody dynamics, *Comput. Methods Appl. Mech. Eng.* 195 (2006) 6891–6908.
- [25] Q. Chen, V. Acary, G. Virlez, O. Brüls, A nonsmooth generalized- $\alpha$  scheme for flexible multibody systems with unilateral constraints, *Int. J. Numer. Methods Eng.* 96 (2013) 487–511.
- [26] O. Brüls, V. Acary, A. Cardona, Simultaneous enforcement of constraints at position and velocity levels in the nonsmooth generalized- $\alpha$  scheme, *Comput. Methods Appl. Mech. Eng.* 281 (2014) 131–161.
- [27] G.A. Costello, *Theory of Wire Rope*, Springer Science & Business Media, 1997.
- [28] L. Meirovitch, *Principles and Techniques of Vibrations*, Prentice Hall, New Jersey, 1997.
- [29] E. Bayo, J.G. De Jalon, M.A. Serna, A modified Lagrangian formulation for the dynamic analysis of constrained mechanical systems, *Comput. Methods Appl. Mech. Eng.* 71 (1988) 183–195.
- [30] J. Chung, G.M. Hulbert, A time integration algorithm for structural dynamics with improved numerical dissipation: the generalized- $\alpha$  method, *J. Appl. Mech.* 60 (1993) 371–375.